The Planetary Science Journal, 3:178 (16pp), 2022 July https://doi.org/10.3847/PSJ/ac7ab8

Lightcurves and Rotations of Trans-Neptunian Objects in the 2:1 Mean Motion Resonance with Neptune

Audrey Thirouin[1] and Scott S. Sheppard[2]
[1] Lowell Observatory, 1400 W. Mars Hill Road, Flagstaff, AZ 86001, USA; thirouin@lowell.edu
[2] Earth and Planets Laboratory, Carnegie Institution for Science, 5241 Broad Branch Road NW, Washington, DC 20015, USA
Received 2022 May 1; revised 2022 June 13; accepted 2022 June 17; published 2022 July 28

Abstract

We report the rotational lightcurves of 21 trans-Neptunian objects (TNOs) in Neptune's 2:1 mean motion resonance obtained with the 6.5 m Magellan-Baade telescope and the 4.3 m Lowell Discovery Telescope. The main survey's goal is to find objects displaying a large lightcurve amplitude that is indicative of contact binaries or highly elongated objects. In our sample, two 2:1 resonant TNOs showed a significant short-term lightcurve amplitude: 2002 VD_{130} and (531074) 2012 DX_{98}. The full lightcurve of 2012 DX_{98} infers a periodicity of 20.80 ± 0.06 hr and amplitude of 0.56 ± 0.03 mag, whereas 2002 VD_{130} rotates in 9.85 ± 0.07 hr with a 0.31 ± 0.04 mag lightcurve amplitude. Based on lightcurve morphology, we classify (531074) 2012 DX_{98} as a likely contact binary but 2002 VD_{130} as a likely single elongated object. Based on our sample and the lightcurves reported in the literature, we estimate the lower percentage of nearly equal-sized contact binaries at only 7%–14% in the 2:1 resonance, which is comparable to the low fraction reported for the dynamically cold classical TNOs. This low contact binary fraction in the 2:1 Neptune resonance is consistent with the lower estimate of the recent numerical modeling. We report the Sloan g', r', and i' surface colors of 2002 VD_{130}, which is an ultra-red TNO whereas 2012 DX_{98} is a very red object based on published surface colors.

Unified Astronomy Thesaurus concepts: Trans-Neptunian objects (1705); Resonant Kuiper belt objects (1396); Twotinos (1727)

Supporting material: machine-readable table

1. Introduction

Located at about 47.7 au, the 2:1 mean motion resonance with Neptune is the second known most populated resonance after Neptune's 3:2 mean motion resonance at ~39.4 au (Volk et al. 2016; Bannister et al. 2018; Chen et al. 2019). The 2:1 Neptune resonance is just beyond the main classical Kuiper Belt and is likely made up of objects that formed in the main classical belt, as well as objects scattered outward from the giant planet region before being trapped into the resonance (Sheppard 2012). The dynamically classical population[3] is trapped between the 3:2 and 2:1 resonances and generally divided between the dynamically hot and cold classical. Typically, the cold classicals have an inclination $i \leqslant 4°$–$5°$, but some works infer that the inclination threshold should be at about 12° (Brown 2001; Elliot et al. 2005; Gladman et al. 2008; Peixinho et al. 2008). Also, Petit et al. (2011) suggested that the cold classical population is composed of at least two subgroups, the stirred and the kernel.

As of 2022 February, the Deep Ecliptic Survey[4] (DES) had classified 106 trans-Neptunian objects (TNOs) confined in the 2:1 resonance. Some objects are classified as likely 2:1 TNOs, but some other classifications (e.g., Centaur or scattered disk object) are also possible based on the currently available astrometry. These objects are 2006 SG_{415},[5] 2009 MG_{10}, 2013 TD_{228}, 2014 SX_{349}, 2014 YZ_{91}, (554102) 2012 KW_{51}, 2016 SJ_{56}, 2017 FD_{163}, and 2017 FQ_{161}.

For decades, lightcurves have been used to estimate the rotational period and lightcurve amplitude, as well as derive the rotational properties (shape, binarity, surface features, and others) of small bodies across the solar system (e.g., Pravec & Harris 2000; Sheppard et al. 2008; Thirouin et al. 2016; Thirouin & Sheppard 2019a). Most TNO lightcurve surveys use small 1–2 m class telescopes and thus are limited to bright objects with, typically, a visual magnitude (V) brighter than ~21 mag (Sheppard et al. 2008; Thirouin et al. 2010). Therefore, there is a bias in the literature toward brighter and thus larger objects, which skews our current understanding of the rotational properties of the TNOs as a population. Recently, several surveys dedicated to the rotational lightcurves of small TNOs were designed using 4–8 m class telescopes to observe TNOs as faint as $V \sim 25$ mag (Thirouin & Sheppard 2018, 2019a; Alexandersen et al. 2019). These new surveys aim to improve our overall understanding of the TNO rotational properties by pushing the facilities to their limit of detectability, but more work has to be done. Observing fainter objects is required, but it is also necessary to increase the number of objects with rotational lightcurves in most of the TNO subpopulations.

Little is known about the rotational characteristics of the 2:1 resonant TNOs. Only four objects (see Section 4.1 for more

[3] For the purpose of this work, our definition of the cold classical population is the same as in Thirouin & Sheppard (2019a).
[4] The DES object classification is available at https://www.boulder.swri.edu/~buie/kbo/desclass.html.
[5] The partial lightcurve of 2006 SG_{415} is presented in this paper. Based on the DES classification, 2006 SG_{415} is likely a 2:1 resonant TNO, but it can also be a scattered disk object. Therefore, care will be taken to include or exclude this object during the presentation and discussion of our results.

details)—(26308) 1998 SM_{165}, (119979) 2002 WC_{19}, (469505) 2003 FE_{128}, and (312645) 2010 EP_{65}—have published rotational lightcurves studies (Romanishin et al. 2001; Sheppard & Jewitt 2002; Kern 2006; Spencer et al. 2006; Sheppard 2007; Benecchi & Sheppard 2013; Thirouin 2013). Three of them have resolved companions, while 2010 EP_{65} is the only one with no satellite detected based on Hubble Space Telescope (HST) images. The satellites of 1998 SM_{165}, 2002 WC_{19}, and 2003 FE_{128} were discovered after their lightcurve studies. Because the lightcurve sample of 2:1 resonant TNOs is extremely limited and biased toward resolved binary systems and bright objects, we aim for this paper to observe faint single 2:1 resonant objects to improve our understanding of this subpopulation. Below, we will describe our survey strategy and target selection. We will also summarize the rotational properties of the 2:1 TNOs and estimate the contact binary percentage in this resonance.

2. Survey Description and Facilities

Our 2:1 Neptune resonance lightcurve survey strategy is inspired by the dynamically cold classical survey published in Thirouin & Sheppard (2019a). The strategy is to image a substantial set of TNOs for partial lightcurves to constrain their rotational periods and amplitudes, as well as to discover interesting objects with a large amplitude (typically, larger than 0.4 mag) that can be indicative of contact binaries or highly elongated objects.

Our first target selection criterion is the visual magnitude. Bright objects ($V \lesssim 22$ mag) are already covered by the literature, and because we are using 4 and 6 m class telescopes, we select objects with a V between ~22 and 23.5–24 mag (more details about facilities below). Preferentially, TNOs without a known resolved companion are chosen, but several of our targets have never been observed with the HST; thus, their resolved binarity status is unknown (see Table 1). Targets are also selected to cover a large range of eccentricities and inclinations (semimajor axis is also considered, but the range is limited due to the definition of the 2:1 resonant population), as well as absolute magnitudes (i.e., sizes). Our selected targets are plotted in Figure 1.

Our survey makes use of two facilities. The Magellan-Baade telescope at Las Campanas Observatory is equipped with IMACS, which is a wide-field imager with eight CCDs giving a 27.′4 diameter field and a pixel scale of 0.″20 $pixel^{-1}$. Our runs at the Lowell Discovery Telescope (LDT), formerly known as Lowell's Discovery Channel Telescope, use the Large Monolithic Imager, which is a 6144 × 6160 pixel CCD with a field of view of 12.′5 × 12.′5 and a pixel scale of 0.″12 $pixel^{-1}$. Exposure times range from 200 to 600 s and are adjusted based on the weather conditions and facility. All observations are obtained with broadband filters (VR and WB4800–7800 filters at LDT and Magellan-Baade, respectively) to maximize the target's signal-to-noise ratio. In one instance, we used the Sloan $g'r'i'$ filters for surface color determination.

All images are calibrated with bias and dome or twilight flats before proceeding with aperture photometry. Once the photometry is on hand, we search for periodicity using the Lomb and phase dispersion minimization techniques (Lomb 1976; Stellingwerf 1978). This series of steps is standard and has been described in greater detail in Thirouin et al. (2010).

3. From Flat to Large Amplitude Lightcurves

3.1. What Is a Lightcurve?

A lightcurve (i.e., brightness variation as a function of time) of a small body is determined by the periodic variation of the body brightness due to its rotation. The two main parameters derived from a lightcurve are (1) the time separation of repeated brightness peaks in the lightcurve, which gives the object's rotational period (P), and (2) the full (or peak-to-peak) lightcurve amplitude (Δm). Rotational period, lightcurve amplitude, and morphology can be used to infer some physical and rotational properties of the body: shape, surface heterogeneity/homogeneity, internal structure, density, and binarity (Sheppard et al. 2008). A lightcurve is due to (1) albedo variation(s) on the object surface, (2) nonspherical shape, and/or (3) binarity (Sheppard et al. 2008). Assuming hydrostatic equilibrium, a small body with a spherical shape is called a MacLaurin spheroid, whereas an elongated triaxial ellipsoidal object is a Jacobi object (Chandrasekhar 1969). As illustrated in Thirouin et al. (2014), a MacLaurin object will have a single-peaked lightcurve whereas a Jacobi or contact binary will display a double-peaked lightcurve. Typically, a spheroidal body with albedo spot(s) on its surface will have a low amplitude lightcurve such as $\Delta m \lesssim 0.15$–0.2 mag. A triaxial ellipsoidal object will have a sinusoidal lightcurve with a moderate lightcurve amplitude of ~0.15–0.2 mag $\lesssim \Delta m \lesssim$ 0.4 mag. The lightcurve of a nearly equal-sized contact binary observed equator-on will have $\Delta m \geqslant 0.9$ mag, and the maximum/minimum of brightness is an inverted U-shape/V-shape from shadowing effects (Lacerda & Jewitt 2007; Lacerda 2011; Lacerda et al. 2014; Harris & Warner 2020). If a contact binary is imaged when the line of sight is further off the equator, the lightcurve will have a lower amplitude, and the V- and U-shapes will be less prominent (Lacerda 2011). Therefore, Thirouin & Sheppard (2019a) used an object with an amplitude greater than 0.9 mag, and the V- and U-shape is a confirmed contact binary. A likely contact binary will have a large amplitude, except that under a 0.9 mag cutoff, and the U- and V-shapes are less prominent (Leone et al. 1984; Lacerda 2011; Descamps 2015). Following Thirouin & Sheppard (2019a), for an object with $\Delta m > 0.4$ mag, we will discuss if it is a likely contact binary or a single triaxial object. We note that ideally, two lightcurves obtained at significantly different epochs are needed for lightcurve modeling purposes to confirm the morphology of the object/system (Lacerda 2011; Lacerda et al. 2014).

In the following, we classify the 21 confirmed 2:1 resonant TNOs (plus 2006 SG_{415}) lightcurves[6] obtained for this work in categories based on their amplitude: (1) a flat lightcurve displays no significant variability, (2) a low amplitude lightcurve has $\Delta m < 0.2$ mag, (3) a moderate amplitude lightcurve with 0.2 mag$< \Delta m <$ 0.4 mag, and (4) a large amplitude lightcurve with $\Delta m > 0.4$ mag.

3.2. Large Amplitude Lightcurves

2002 VD_{130}—This object was observed on several occasions with the LDT from 2019 to 2021 (Figure 2). The Lomb periodogram inferred a rotational period of 4.87 cycles day^{-1} (or 4.93 hr), but there are several nearby aliases with a high

[6] Photometry and partial/flat lightcurves are available in Appendix and Table 3.

Table 1
Observing Log with the Date of Observations (UT-obs), Number of Images (N), Heliocentric and Geocentric Distances (r_h and Δ), and Phase Angle (α) for Our Runs

TNO	UT-obs	N	r_h (au)	Δ (au)	α (°)	Filter	Telescope	Period (hour)	Amplitude (mag)	$H_{\rm MPC}$ (mag)	a (au)	e	i (°)	Binary[c] Yes/No/?
(137295) 1999 RB_{216}	9/20/2020	9	33.091	33.851	1.1	VR	LDT	>6	>0.15	7.3	47.814	0.297	12.7	No
2000 QL_{251}	10/6/2019	8	39.782	40.773	0.2	VR	LDT	>6	>0.15	6.8	47.935	0.220	3.7	Yes
(524179) 2001 FQ_{185}	5/16/2018	9	37.002	36.033	0.5	WB	Magellan	~6.8	~0.06	6.9	47.762	0.230	3.2	No
2001 UP_{18}	9/24/2020	10	50.198	51.011	0.7	VR	LDT	>5	>0.2	6.0	47.719	0.080	1.2	?
	10/17/2020	7	50.056	51.027	0.3	VR	LDT	⋯	⋯	⋯	⋯	⋯	⋯	⋯
2002 PU_{170}	9/20/2020	7	42.469	43.460	0.2	VR	LDT	⋯	~0.1	7.1	47.835	0.220	1.9	?
2002 VD_{130}[a]	12/19/2019	8	31.461	32.419	0.4	VR	LDT	9.85	0.31 ± 0.04	7.5	47.324	0.317	3.9	No
	2/2/2020	6	31.602	32.424	1.0	VR	LDT	⋯	...	...	...	...	...	...
	9/20/2020	6	32.704	32.454	1.7	gri, VR	LDT	...	...	...	...	...	...	...
	12/22/2020	19	31.505	32.468	0.4	VR	LDT	...	...	...	...	...	...	...
	1/18/2021	12	31.530	32.472	0.5	VR	LDT	...	...	...	...	...	...	...
2003 UP_{292}	12/6/2019	3	27.936	28.900	0.4	VR	LDT	>1	>0.1	7.3	47.559	0.414	13.0	?
	12/19/2019	4	27.949	28.907	0.4	VR	LDT	...	...	...	...	...	...	...
2004 HP_{79}	5/22/2018	5	38.877	37.884	0.3	VR	LDT	>3	>0.29	6.6	48.030	0.191	2.2	?
	5/20/2020	5	37.852	38.858	0.2	VR	LDT	...	...	...	...	...	...	...
2004 TV_{357}	10/3/2019	6	34.397	34.806	1.5	VR	LDT	⋯	~0.1	6.9	47.433	0.273	9.8	No
	10/6/2019	7	34.351	34.805	1.5	VR	LDT	...	...	...	...	...		...
	2/14/2020	5	34.441	34.779	1.5	VR	LDT	...	...	...	...	...		...
(470083) 2006 SG_{369}	10/3/2019	9	30.802	31.375	1.5	VR	LDT	>4.5	>0.38	7.6	48.011	0.373	13.6	No
	10/6/2019	7	30.763	31.376	1.5	VR	LDT	>5	>0.08	...	...	...	...	...
2011 EY_{90}	5/20/2020	5	35.315	36.143	0.9	VR	LDT	⋯	~0.1	7.0	47.986	0.264	8.0	?
(531074) 2012 DX_{98}[a]	5/16/2018	8	35.119	34.306	1.0	WB	Magellan	20.80	0.56 ± 0.03	7.3	47.916	0.267	13.1	?
	5/17/2018	5	35.119	34.316	1.0	WB	Magellan	...	...	...	...	...	...	...
	5/18/2018	10	35.119	34.327	1.0	WB	Magellan	...	...	...	...	...	...	...
	5/19/2018	11	35.119	34.337	1.1	WB	Magellan	...	...	...	...	...	...	...
	5/22/2018	10	35.119	34.370	1.1	VR	LDT	...	...	...	...	...	...	...
	2/28/2019	6	34.486	35.123	1.1	WB	Magellan	...	...	...	...	...	...	...
	3/1/2019	6	34.375	35.123	1.1	WB	Magellan	...	...	...	...	...	...	...
	3/2/2019	6	34.363	35.123	1.0	WB	Magellan	...	...	...	...	...	...	...
(554102) 2012 KW_{51}	5/19/2020	8	38.738	39.715	0.4	VR	LDT	>5	>0.12	6.5	47.926	0.242	11.7	?
2012 WE_{37}	9/20/2020	5	35.533	36.175	1.2	VR	LDT	⋯	~0.1	7.8	47.837	0.249	25.7	?
2012 XR_{157}	11/30/2019	4	39.495	40.414	0.5	WB	Magellan	⋯	~0.1	6.4	47.538	0.222	30.0	?
	12/1/2019	7	39.492	40.413	0.5	WB	Magellan	...	...	...	...	...	...	...
	2/14/2020	3	40.008	40.377	1.3	VR	LDT	...	...	...	...	...	...	...

Table 1
(Continued)

TNO	UT-obs	N	r_h (au)	Δ (au)	α (°)	Filter	Telescope	Period (hour)	Amplitude (mag)	H_{MPC} (mag)	a (au)	e	i (°)	Binary[c] Yes/No/?
(577578) 2013 GW_{136}	5/19/2020	6	30.850	31.857	0.2	VR	LDT	>4	>0.17	7.6	47.929	0.347	6.7	?
	5/20/2020	3	30.852	31.857	0.2	VR	LDT	...	...	...	...	...	...	...
2013 TG_{172}	9/20/2020	8	32.591	33.506	0.7	VR	LDT	⋯	∼0.1	8.2	48.322	0.326	4.8	?
2014 GE_{54}	5/18/2018	6	38.715	37.824	0.7	WB	Magellan	>4	>0.1	6.6	48.006	0.259	17.0	?
(534626) 2014 UT_{224}	11/19/2019	3	34.662	35.622	0.4	VR	LDT	>3.5	>0.1	6.7	48.041	0.267	3.9	?
	12/19/2019	6	34.687	35.629	0.5	VR	LDT	...	...	...	...	...		...
	2/14/2020	3	35.385	35.642	1.5	VR	LDT	...	...	...	...	...	...	...
(535025) 2014 WT_{509}	12/02/2019	7	34.969	35.935	0.3	WB	Magellan	>5	>0.26	7.2	47.617	0.255	12.3	?
	12/19/2019	7	35.024	35.939	0.6	VR	LDT	...	...	...	...	...	...	...
	9/24/2020	6	35.658	36.007	1.5	VR	LDT	...	...	...	...	...	...	...
	10/17/2020	5	35.341	36.012	1.2	VR	LDT	...	...	...	...	...	...	...
2017 DN_{121}	2/14/2020	10	36.335	37.312	0.2	VR	LDT	>5	>0.1	7.4	47.493	0.223	15.2	?
2006 SG_{415}[b]	10/6/2019	8	32.981	33.976	1.2	VR	LDT	⋯	∼0.1	7.8	48.360	0.298	31.3	?

Notes. The last column presents any hints of a resolved wide binary based on HST observations: (1) objects with a satellite detected are indicated with "yes," (2) objects with no detected moon are indicated with "no," and (3) a question mark means that an object has not been observed with the HST and thus we do not know if it has a resolved companion. We also summarize our results regarding rotational period and lightcurve amplitude.

[a] Object 2012 DX_{98} is classified as a likely contact binary. The current lightcurve of 2002 VD_{130} favors an elongated single object.

[b] Object 2006 SG_{415} is likely a 2:1 resonant TNO, but additional astrometry can favor/discard a scattered disk object orbit.

[c] The discovery of the binarity of 2001 QL_{251} was reported in Noll et al. (2006). Several HST programs were awarded to search for satellites and/or derive colors—Nos. 11113 (PI: Noll), 11644 (PI: Brown), and 12234 (PI: Fraser)—but no moons were detected.

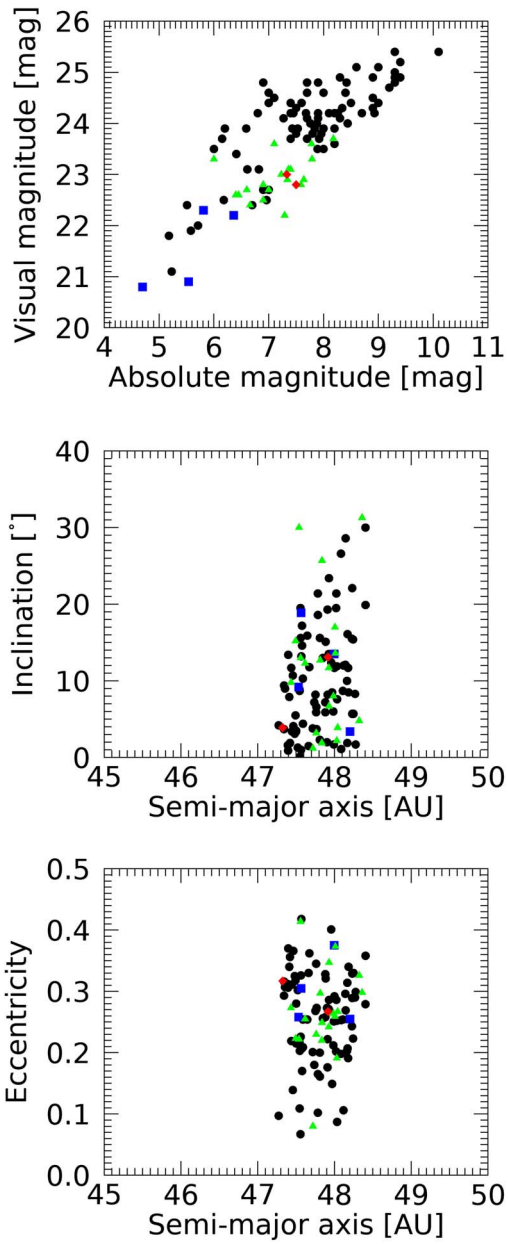

Figure 1. The 2:1 resonant TNOs are classified into four groups: (1) objects with a lightcurve from the literature (blue squares; see Section 4.1 for more details), (2) objects with a flat-to-moderate lightcurve amplitude from our survey (green triangles), (3) objects with a large amplitude from this survey (red diamonds), and (4) objects never observed for lightcurve study (black circles). Our survey is combined with published lightcurves of 2:1 TNOs to cover a range of inclination, eccentricity, and absolute magnitude. Note that the nine likely 2:1 TNOs mentioned in the Introduction are plotted. Orbital elements and absolute and visual magnitudes are from the Minor Planet Center (2022 February).

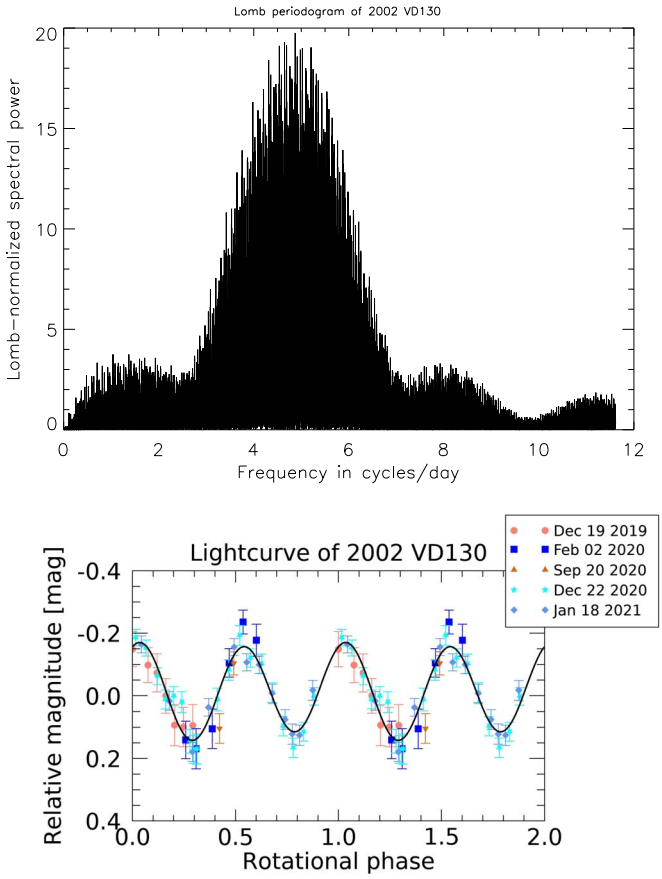

Figure 2. The Lomb periodogram (upper plot) favors a rotational frequency at 4.87 cycles day^{-1}. Due to the large amplitude and asymmetric lightcurve, the double-peaked rotational lightcurve with a periodicity of 9.85 hr is favored (lower plot). A second-order Fourier fit is overplotted (black line).

confidence level as well. Due to the large amplitude and asymmetric lightcurve with the first minimum being deeper than the second one, the double-peaked rotational period is favored. The rotational period of 2002 VD_{130} is about 9.85 ±0.07 hr, and the full lightcurve amplitude is 0.31 ± 0.04 mag from the second-order Fourier fit. The lightcurve of 2002 VD_{130}displays a large amplitude, but there is no sign of the characteristic V-shape and U-shape of a contact binary. The sinusoidal morphology of this lightcurve would currently suggest that 2002 VD_{130} is an elongated object and not a clear contact binary candidate. Future observations at a significantly later epoch will help determine the true nature of this object, but for now, we do not classify 2002 VD_{130} as a candidate contact binary TNO.

Following the formalism described in Chandrasekhar (1987), one can derive the axis ratio and lower limit to the density of an ellipsoidal object in hydrostatic equilibrium for a given rotational period. If 2002 VD_{130} is an elongated Jacobi body with axes such as $a > b > c$ and is rotating along its c-axis, its density is $\rho \geqslant 0.42$ g cm^{-3}, and the axis ratios are $a/b = 1.46$ and $c/a = 0.47$, assuming that this object was observed under an equatorial view. If we consider that the lightcurve of 2002 VD_{130} is single-peaked, then its rotational period is 4.93 hr (half the period of the double-peaked lightcurve), and in this case, the lower limit to the density would be 1.69 g cm^{-3}. Grundy et al. (2012) reported the densities of several binary/multiple systems that were extracted from their mutual orbitals and mass determinations. Based on Figure 7 in Grundy et al. (2012), there is a clear trend inferring that small objects have densities lower than 1 g cm^{-3}, whereas large objects have densities above 1 g cm^{-3} limit. Object 2002 VD_{130} has a diameter between ∼100 and ∼200 km (assuming an albedo of 0.20 and 0.04, respectively); therefore, its density is likely below or around 1 g cm^{-3}. Therefore, we can rule out the density estimate derived from the single-peaked lightcurve, and also clearly favor the double-peaked lightcurve.

(531074) 2012 DX_{98}—This object was observed seven times with the Magellan-Baade telescope and during 1 night with the

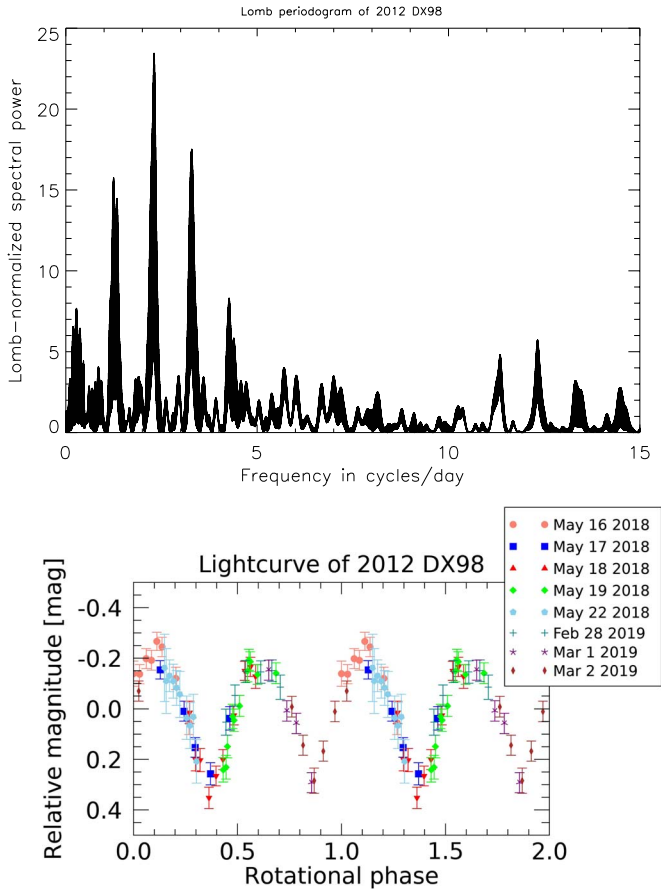

Figure 3. The main peak favored by the Lomb periodogram is at 2.31 cycles day^{-1} (10.40 hr). Due to the large amplitude and assymetric lightcurve, we choose the double-peaked period of 2 × 10.40 hr = 20.80 hr.

LDT between 2018 May and 2019 March. The Lomb periodogram in Figure 3 favors a single-peaked period of 2.31 cycles day^{-1} (i.e., 10.40 hr) but a double-peaked rotational period of 20.80 hr, and an amplitude of 0.56 mag is preferred (Figure 3). The lightcurve morphology with the V- and U-shapes is characteristic of a contact binary from the shadowing effects of the two components. However, the lightcurve amplitude is below the threshold generally used to classify an object as a nearly equal-sized contact binary (Sheppard & Jewitt 2004). So, following the terminology used in Thirouin & Sheppard (2019a), we consider 2012 DX_{98} as a likely contact binary, as future observations will determine if the amplitude gets larger as the object becomes viewed more equator-on.

If 2012 DX_{98} is a contact binary, its mass ratio is between $q_{\rm max} = 0.53$ with $\rho_{\rm max} = 5$ g cm^{-3} and $q_{\rm min} = 0.47$ with $\rho_{\rm min} = 1$ g cm^{-3}. Because $q_{\rm min}$ and $q_{\rm max}$ are comparable, we consider the case where $q = 0.5$ and $\rho = 1$ g cm^{-3} to estimate that the axis ratios for the primary are $b_p/a_p = 0.97$ and $c_p/a_p = 0.94$, and those for the secondary are $b_s/a_s = 0.93$ and $c_s/a_s = 0.91$, while the separation between the two components is $D = 0.48$, corresponding to 252/113 km (with an albedo of 0.04/0.20).

Even if the contact binary configuration is favored, we also consider the case of a single elongated object to estimate that the density should be larger than 0.10 g cm^{-3} for a body with $a/b = 1.67$ and $c/a = 0.43$ (Chandrasekhar 1987).

3.3. Moderate Amplitude Lightcurves

2004 HP_{79}—In about 3 hr of observations, 2004 HP_{79} has a variability of 0.29 mag. We do not have enough data to derive a rotational period.

(470083) 2006 SG_{369}—This object was observed over 2 nonconsecutive nights in 2019 October over 4.5 and 5 hr, respectively. The variability is not consistent over the two observing blocks, as we reported a variability of 0.38 and 0.08 mag. After a detailed inspection of our data set, there is no obvious background contamination able to explain such different amplitudes. Therefore, we considered that both runs tested different phases of the lightcurve, possibly indicating a very long period for this object. For the following statistical analysis, we will use a mean amplitude of 0.23 mag.

(55025) 2014 WT_{509}—Based on 1 isolated night at the Magellan telescope, we report a moderate lightcurve amplitude of 0.26 mag over 5 hr of observations. We reobserved this object at the LDT, but the weather, as well as technical difficulties, resulted in low-quality data. Therefore, for our study, we will only consider the results from the Magellan-Baade lightcurve.

3.4. Flat and Low Amplitude Lightcurves

(137295) 1999 RB_{216}—In about 6 hr, this object presents an amplitude of ∼0.12 mag. We imaged a minimum and part of the maximum in 1 night; therefore, we constrain the rotational period to be about 6/12 hr assuming a single-/double-peaked option.

2000 QL_{251}—This object is the only known resolved binary observed during our survey. The variability is low, about 0.15 mag over 6 hr.

(524179) 2001 FQ_{185}—We report a consecutive maximum and minimum during our observations allowing us to constrain the rotational period to ∼6.8 hr, while the amplitude is ∼0.06 mag.

2001 UP_{18}—Based on about 5 hr of observations under variable weather conditions, we report an amplitude likely lower than or near 0.2 mag for this object.

2003 UP_{292}—We only have a few images for the above reasons and can only conclude that the object's variability was low, over about 1 hr.

2012 KW_{51}—In approximately 5 hr, 2012 KW_{51} displayed a variability of ∼0.12 mag.

2013 GW_{136}—This body was observed over 2 consecutive nights at the LDT. Because we only obtained two usable images on the second night, the period and amplitude constraints are based on the first night. The period of 2013 GW_{136} is longer than 4 hr, and the amplitude is likely greater than 0.17 mag.

2014 GE_{154}—Based on ∼4 hr of observations with the Magellan-Baade telescope over 1 night, the variability of 2014 GE_{154} is only ∼0.1 mag. This data set alone is insufficient to derive the periodicity of this object.

(534626) 2014 UT_{224}—In 3 isolated nights, we observed this object under variable conditions; thus, we only report a handful of images suggesting an amplitude larger than 0.1 mag over 3.5 hr.

2017 DN_{121}—With only 1 night of data for 2017 DN_{121}, we can only infer that the variability of this object is low, around 0.1 mag in 5 hr.

Table 2
Published Lightcurves of Four 2:1 Resonant TNOs with Information Regarding Rotational Period, Lightcurve Amplitude and Absolute Magnitude Summarized

Object	Single-peaked P (hr)	Double-peaked P (hr)	Δm (mag)	$H_{\rm MPC}$ (mag)	References[a]
(26308) 1998 SM_{165}[b]	...	7.966	0.56	5.8	R01
	...	7.1	0.45	...	S02
	...	8.40 ± 0.05	0.56	...	S06
(119979) 2002 WC_{19}[b]	...	...	<0.05	4.7	S07
	...	...	<0.10	...	T13
(469505) 2003 FE_{128}[b]	5.85 ± 0.15	...	0.50 ± 0.14	6.4	K06
(312645) 2010 EP_{65}[c]	7.48	14.97	0.17 ± 0.03	5.5	B13

Notes.
[a] References list: R01, Romanishin et al. (2001); S02, Sheppard & Jewitt (2002); K06, Kern (2006); S06, Spencer et al. (2006); S07, Sheppard (2007); B13, Benecchi & Sheppard (2013); T13, Thirouin (2013).
[b] Known resolved wide binaries: Brown & Trujillo (2002); Noll et al. (2007), http://www2.lowell.edu/users/grundy/tnbs/469505_2003_FE128.html. Object 2010 EP_{65} was observed by HST program 12468 (PI: K. S. Noll), and no satellite was discovered.
[c] Several aliases are reported by Benecchi & Sheppard (2013).

2002 PU_{170}, 2004 TV_{357}, 2006 SG_{415}, 2011 EY_{90}, 2012 WE_{37}, 2012 XR_{157}, and 2013 TG_{172}—Objects 2002 PU_{170}, 2006 SG_{415}, 2011 EY_{90}, 2012 WE_{37}, 2012 XR_{157}, and 2013 TG_{172} were observed over 1 or 2 observing nights, and they all displayed a very low variability. The only known 2:1 resonant TNO with neutral surface colors according to Sheppard (2012), 2004 TV_{357}, was scheduled for observations over 3 nonconsecutive nights with the LDT in 2019 and 2020. Over this amount of time, the lightcurve amplitude was very low.

4. Rotational Properties

4.1. Lightcurves from the Literature

Only four bright 2:1 resonant TNOs have significant time-resolved photometric information in the literature (Table 2 and Figure 1). Three of them are known resolved binary systems; thus, the published lightcurves are the system's lightcurves because the components are unresolvable with ground-based observations.

Sheppard (2007) observed 2002 WC_{19} over 3 nights in 2003 December with observing blocks of about 6, 3, and 5.5 hr and reported a nearly flat lightcurve. Based on data obtained over 3 nights in 2004 January, Thirouin (2013) also concluded that 2002 WC_{19} has a nearly flat lightcurve with an amplitude less than 0.10 mag. Benecchi & Sheppard (2013) reported several potential rotational periods for 2010 EP_{65}, but it seems that the best fit is obtained for a double-peaked lightcurve with a rotational period of 14.97 hr and an amplitude of 0.17 mag. Kern (2006) presented 18 images obtained over 1 observing night of 2003 FE_{128}. A single-peaked lightcurve with a rotational period of 5.85 hr and amplitude of 0.50 mag was derived. Unfortunately, less than half of the single-peaked lightcurve was covered during the observing time. Based on Figure 20 of Kern (2006), the amplitude of the data set is only about 0.25 mag, as that is the maximum amplitude actually observed. The 0.50 mag inferred by Kern (2006) is based on the lightcurve fit but as the maximum of the curve is missing, it is unclear if the fit is realistic. We use an amplitude of 0.25 mag for this object. Also, because of the moderate to potentially large amplitude, the double-peaked lightcurve is maybe a better option compared to the single-peaked one (Thirouin et al. 2014). For this work, we used the double-peaked lightcurve with a period of 11.70 hr. Additional data to confirm the amplitude and secure the rotational period are warranted.

Several lightcurves of 1998 SM_{165} have been published. The first lightcurve was obtained by Romanishin et al. (2001); they favored a period of 7.966 hr and amplitude of 0.56 mag based on 4 nights of data in 1999 and 2000. However, Spencer et al. (2006) inferred a period of 8.40 hr using 3 nights from 2005 December. The amplitude is consistent with the Romanishin et al. (2001) result, and a period of 8.40 hr appears to adequately fit the Romanishin et al. (2001) and Spencer et al. (2006) data sets (J. Spencer, private communication). Sheppard & Jewitt (2002) obtained a partial lightcurve suggesting an amplitude of at least 0.45 mag and a period of at least 7.1 hr. Here we will use the period and amplitude estimated by Spencer et al. (2006).

Finally, several similarities between 1998 SM_{165} and 2006 SG_{369} are highlighted. Both objects have similar orbital elements,[7] and they might both display large lightcurve amplitudes (see this section and Section 3). Also, they have similar surface colors with $g' - r' = 0.91 \pm 0.04$ and $g' - i' = 1.31 \pm 0.03$ mag for 2006 SG_{369} according to Sheppard (2012), and the colors[8] of 1998 SM_{165} are $g' - r' = 0.90 \pm 0.05$ and $g' - i' = 1.34 \pm 0.07$ mag from Delsanti et al. (2001). Such similar orbital elements and surface colors may indicate that these objects are a pair (Vokrouhlický & Nesvorný 2008; Abedin et al. 2021). Numerical modeling is warranted to confirm such a find.

4.2. Lightcurves from Our Survey

Our survey observed 21 2:1 resonant TNOs (22 TNOs if 2006 SG_{415} is included). The TNO 2000 QL_{251} is a binary system (Noll et al. 2006), but the satellite is not resolved in our images; thus, we report the combined lightcurve of the primary and secondary. Four TNOs were observed with HST and have no detected moon: 2001 FQ_{185}, 2002 VD_{130}, 2004 TV_{357}, and 2006 SG_{369}. The other TNOs have never been observed for binarity using HST, so their binarity status is unclear.

Most of the lightcurves reported in this work are partial, as our main goal is to identify high amplitude lightcurves and thus

[7] Orbital parameters computed by the Minor Planet Center for 1998 SM_{165} and 2006 SG_{369} are at https://minorplanetcenter.net/db_search/show_object?object_id = 470083 and https://minorplanetcenter.net/db_search/show_object?object_id = 26308.
[8] The *BVRI* colors reported in Delsanti et al. (2001) were converted to $g'r'i'$ using the equations from Smith et al. (2002).

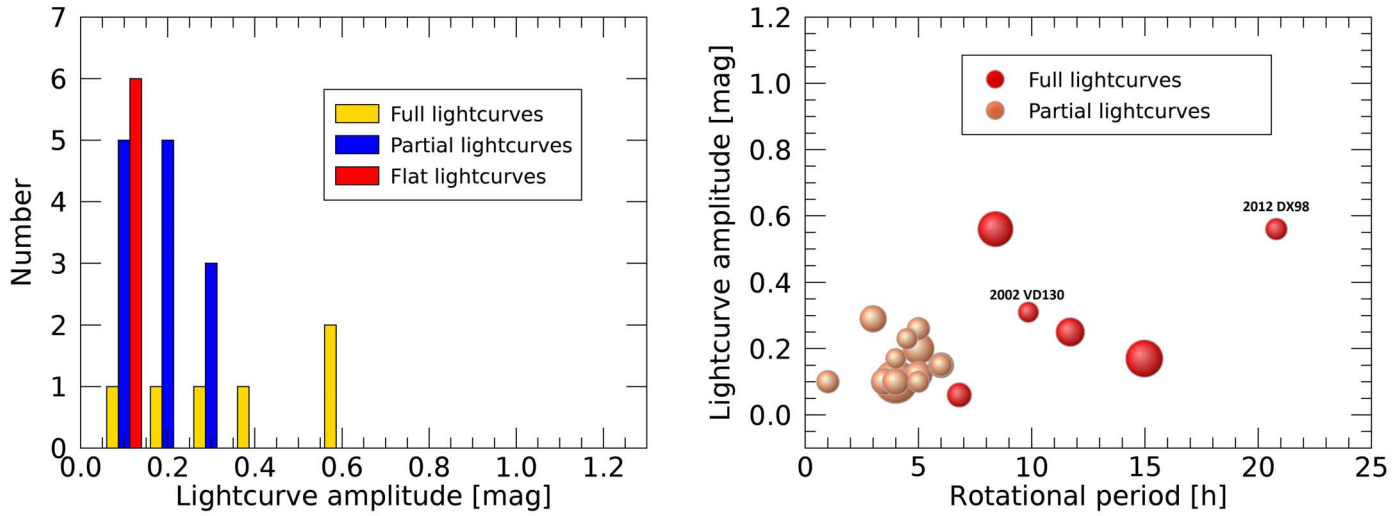

Figure 4. We summarize the number of partial, flat, and full in the 2:1 resonance (left plot). On the right, the bubble size varies with the object's absolute magnitude. There is no obvious trend between lightcurve variability and absolute magnitude. Binaries display a larger amplitude than single objects. The two large amplitude TNOs found by our survey are indicated.

potential contact binaries for future more intensive observations. Only the lightcurve of 2001 FQ_{185} is nearly complete, as this object has a rotational period consistent with the observing time spent on this object. Our survey found one likely contact binary, 2012 DX_{98}, and one single elongated object, 2002 VD_{130}.

4.3. Amplitude and Period Distributions

The literature and our survey report six full lightcurves, 12 partial lightcurves, and seven flat (excluding the flat lightcurve of 2006 SG_{415}). Two 2:1 TNOs have large amplitudes, the likely contact binary 2012 DX_{98} and the known resolved binary 1998 SM_{165} (Figure 4). The average amplitude is 0.32 mag for the full lightcurves and 0.16 mag for the partial lightcurves. The mean rotational period of the binary systems is about 13.6 hr. There are not enough full lightcurve of single objects to estimate the median period, but it seems that the binaries tend to rotate slower than the single objects in other dynamical populations (Thirouin et al. 2014; Thirouin & Sheppard 2018, 2019a).

4.4. Resolved and Unresolved Binaries

From this work, 2012 DX_{98} is likely a nearly equal-sized contact binary, whereas the lightcurve of 2002 VD_{130} is best interpreted as a single triaxial object. But the case of 1998 SM_{165} has to be discussed in more detail. Object 1998 SM_{165} has a large lightcurve amplitude of 0.56 mag (i.e., the same amplitude as 2012 DX_{98}), but the lightcurve does not present the typical U- and V-shapes of a contact binary (Romanishin et al. 2001; Spencer et al. 2006). The lightcurve interpretation proposed by Romanishin et al. (2001) is that 1998 SM_{165} is an irregularly shaped object. Since the lightcurve's publication, a small satellite has been discovered orbiting 1998 SM_{165} (Grundy et al. 2011). To summarize, based on the large lightcurve amplitude of 1998 SM_{165}, it could be a contact binary, but the lightcurve is not displaying the usual V- and U-shapes; thus, the lightcurve interpretation is still open to debate. Below, we will consider 1998 SM_{165} as a contact binary and an elongated object.

Sheppard & Jewitt (2004) estimated the fraction of contact binaries in the trans-Neptunian population using the following approach. The lightcurve amplitude of a small body with axis such as $a > b$ and $b = c$ varies with the angle of the object's pole relative to the perpendicular of the line of sight (θ),

$$\Delta_m = 2.5 \log\left(\frac{1 + \tan\theta}{(b/a) + \tan\theta}\right), \quad (1)$$

whereas the lightcurve amplitude of a triaxial ellipsoid varies as

$$\Delta_m = 2.5 \log\left(\frac{a}{b}\right) - 1.25 \log\left[\left(\left(\frac{a}{b}\right)^2 - 1\right)\sin^2\theta + 1\right]. \quad (2)$$

Using Equation (1) and considering that an object with $a/b = 3$ (corresponding to a contact binary) has a lightcurve amplitude of 0.5 mag, we compute that θ has to be $\sim$36°. The probability that Earth would lie within 36° of the equator of randomly oriented objects is $P(\theta \leqslant 36°) \sim 0.59$. Using the same axis ratio and amplitude cutoff, Equation (2) infers $\theta \sim 34.^{\circ}5$ and $P(\theta \leqslant 34.^{\circ}5) \sim 0.57$. The amplitude cutoff of 0.5 mag was chosen based on the lightcurve amplitudes of 2012 DX_{98} and 1998 SM_{165}.

Excluding 2006 SG_{415} from our sample (because its dynamical classification is uncertain), we have a total of 25 objects observed for lightcurve studies. Assuming that 2012 DX_{98} is the only contact binary in the 2:1 resonance, the fraction of contact binaries is $f(\Delta m \geqslant 0.5 \text{ mag}) \sim 1/(25 \times P(\theta)) \sim 7\%$ (same result with Equations (1) and (2)). Including 1998 SM_{165} as a contact binary, we estimate that $f(\Delta m \geqslant 0.5 \text{ mag}) \sim 2/(25 \times P(\theta)) \sim 14\%$ using the previous equations. Therefore, we report a nearly equal-sized contact binary fraction at $\sim$7%–14% for the 2:1 resonance with Neptune. This is only a lower limit because of possible projection effects. Some nearly equal-sized contact binaries would still only show low amplitude lightcurves when observed near pole-on.

Noll et al. (2020) reported that the fraction of 2:1 resolved binaries with $i < 12°$ and an absolute magnitude between 5 and 8 mag is 27^{+16}_{-9}%, which is higher than the 5^{+6}_{-2}% estimate for the 3:2 resonance but similar to the fraction of resolved binaries

in the dynamically cold classicals at 29^{+7}_{-6}%. Noll et al. (2020) also pointed out that the resolved binaries tend to be at higher inclinations in the 3:2 resonance. The use of the widely separated equal-sized systems in the trans-Neptunian belt to constrain Neptune's migration was proposed by Murray-Clay & Schlichting (2011). If the migration-induced capture scenario is favored, some of the testable outcomes are (1) the 2:1 and 3:2 mean motion resonances with Neptune should have a low-inclination cold classical component, and (2) the low-inclination group in the 2:1 resonance should have a higher binary fraction than the high-inclination counterpart, whereas the 3:2 low-inclination component should have a fraction ∼20%–30% lower than the cold classicals. Sheppard (2012) demonstrated that both resonances have a cold classical component at low inclination based on color measurements, and the wide binary fractions reported by Noll et al. (2020) are also in agreement with a migration-induced capture scenario. Contact binaries are not considered by Murray-Clay & Schlichting (2011), but they are also at low-to-moderate inclinations (<20°) in the 3:2 and 2:1 resonances (Thirouin & Sheppard 2018). However, the higher fraction of contact binaries is in the 3:2 and not the 2:1, as for the wide binaries.

Thirouin & Sheppard (2018) reported a nearly equal-sized contact binary fraction of ∼40%–50% (corrected from projection effects) for the 3:2 mean motion resonance, and Thirouin & Sheppard (2019a) inferred a fraction up to ∼10%–25% (corrected from projection effects) for the dynamically cold classical. Therefore, the estimate for the 2:1 resonance is even lower than for the cold classical population, but as our 2:1 sample is smaller than the cold classical one, we will consider that the estimates for these two subpopulations are similarly low compared to the 3:2 resonance. Nesvorný & Vokrouhlický (2019) predicted a contact binary fraction between 10% and 30% for the excited TNO populations (as the 2:1 resonance); therefore, our fraction is consistent with the lower range of the modeling estimate. The Nesvorný & Vokrouhlický (2019) model only considers the collapse of a wide binary as the genesis of a contact binary, which is not the only proposed mechanism to create these systems (Goldreich et al. 2002; Weidenschilling 2002; Nesvorný et al. 2010; Porter & Grundy 2012; Nesvorný & Vokrouhlický 2019). Also, the modeling is not focused on each TNO subpopulation but rather on the cold classicals versus the excited populations. Therefore, there is a clear need for additional modeling efforts to understand the formation of contact binaries and their fractions across the trans-Neptunian belt.

The different contact binary fractions can also be due to the past history and interactions with Neptune of these three subpopulations (e.g., Parker & Kavelaars 2010; Nesvorný 2015; Nesvorný & Vokrouhlický 2019; Volk & Malhotra 2019; Morbidelli & Nesvorný 2020). The cold classical population had very limited interactions with Neptune, whereas the 3:2 was sculpted by these interactions. The 2:1 resonant objects were also likely affected by Neptune interactions in order to get them into resonance, but they present a low ratio of contact binaries, which is unlike the 3:2 resonance but similar to the cold classicals. This may suggest that the 2:1 resonance Neptune interactions were not as strong as the 3:2 resonance Neptune interactions, as the 2:1 also has a large number of wide binaries, again similar to the less dynamically stirred cold classicals and unlike the 3:2 resonance population. More simulations of how the contact binaries form through Neptune's interactions and/or migration is warranted.

4.5. Colors of Large Amplitude Objects in the 2:1 Resonance

Three objects, 1998 SM_{165}, 2002 VD_{130}, and 2012 DX_{98}, have large lightcurve amplitudes from 0.31 to 0.56 mag.

Based on surface color measurements, 1998 SM_{165} is an ultra-red object (Delsanti et al. 2001; Peixinho et al. 2015). Thirouin & Sheppard (2019b) evaluated that the Sloan $g'r'i'$ surface colors of 2012 DX_{98} are $g' - r' = 0.85 \pm 0.06$ and $g' - i' = 1.25 \pm 0.06$ mag. Based on its very red colors, which are typical of the dynamically cold classical population, Thirouin & Sheppard (2019b) suggested that 2012 DX_{98} is potentially an escaped cold classical.

On 2020 September 20 UT, the $g'r'i'$ colors of 2002 VD_{130} were derived using the LDT. Its colors are $g' - r' = 1.03 \pm 0.06$ and $g' - i' = 1.35 \pm 0.06$ mag, which correspond to an ultra-red object. Therefore, all three objects with a large lightcurve amplitude have similar surface colors possibly linking them to the dynamically cold classicals (Thirouin & Sheppard 2019b).

5. Summary and Conclusions

The main results of this work are as follows.

1. We report the short-term variability of 21 2:1 resonant TNOs. With our survey and the literature, we compile 18 TNOs showing a low-to-high lightcurve amplitude.
2. We propose the first lightcurve of 2012 DX_{98}, which rotates in ∼21 hr and has a large amplitude of 0.56 mag. Based on its lightcurve morphology, 2012 DX_{98} is likely a contact binary whose mass ratio is about 0.5.
3. The lightcurve of 2002 VD_{130}, with an amplitude of ∼0.3 mag and periodicity of 9.85 hr, seems to be due to a single elongated object.
4. The contact binary fraction in the 2:1 resonance is very low, ∼7%–14%, which is similar to the fraction in the cold classical population. Modeling from Nesvorný & Vokrouhlický (2019) suggested that excited TNO populations should have a fraction of contact binaries of 10%–30%. Therefore, estimates based on observations are consistent with the lower limit of the modeling results.
5. The surface $g'r'i'$ colors of 2002 VD_{130} and 2012 DX_{98} are very red/ultra-red which is consistent with an origin in the dynamically cold classical population (Thirouin & Sheppard 2019b).

We thank two anonymous reviewers for their careful reading of this work. This paper includes data gathered with the 6.5 m Magellan-Baade telescope located at Las Campanas Observatory, Chile. This research is based on data obtained at the Lowell Discovery Telescope (LDT; previously known as the Discovery Channel Telescope, DCT). Lowell Observatory is a private, nonprofit institution dedicated to astrophysical research and public appreciation of astronomy and operates the LDT in partnership with Boston University, the University of Maryland, the University of Toledo, Northern Arizona University, and Yale University. Partial support of the LDT was provided by Discovery Communications. The LMI was built by Lowell Observatory using funds from the National Science Foundation

(AST-1005313). The authors acknowledge the LDT and Magellan staffs. The authors also acknowledge support from National Science Foundation (NSF) grant Nos. AST-1734484 awarded to the "Comprehensive Study of the Most Pristine Objects Known in the Outer Solar System" and AST-2109207 awarded to the "Resonant Contact Binaries in the Trans-Neptunian Belt."

Facilities: Lowell Discovery Telescope (LDT), Magellan-Baade Telescope.

Appendix

The sparse lightcurves discussed in this paper are given in Figure 5.

The photometry of all targets observed in this paper is available in Table 3. No light-time correction is applied. Clinical Education Coordinator at Lehigh Valley Health Network.

Table 3
The Photometry of All Targets Observed in This Paper. No Light-time Correction is Applied.

TNO	Julian Date	Relative Magnitude (mag)	Error (mag)
1999 RB_{216}			
	2,459,112.74797	−0.07	0.04
	2,459,112.76947	0.01	0.04
	2,459,112.79098	0.05	0.04
	2,459,112.81929	0.08	0.04
	2,459,112.84876	0.01	0.03
	2,459,112.87824	−0.07	0.03
	2,459,112.90750	−0.05	0.03
	2,459,112.93563	−0.07	0.03
	2,459,113.00314	0.00	0.04

Note. Table 3 is published in its entirety in the electronic edition of the journal. A portion is shown here for guidance regarding its form and content.

(This table is available in its entirety in machine-readable form.)

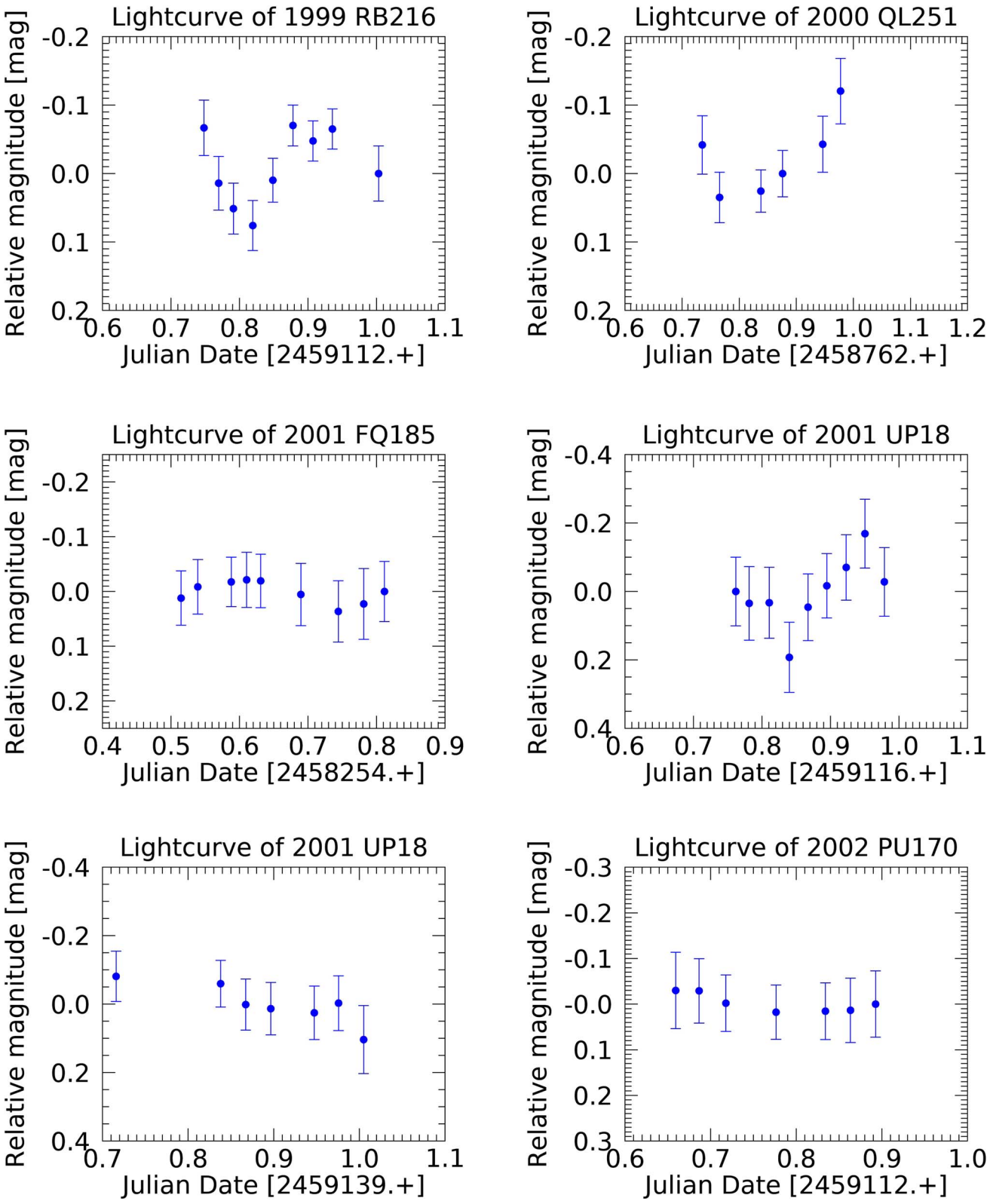

Figure 5. Objects in the 2:1 mean-motion resonance with Neptune.

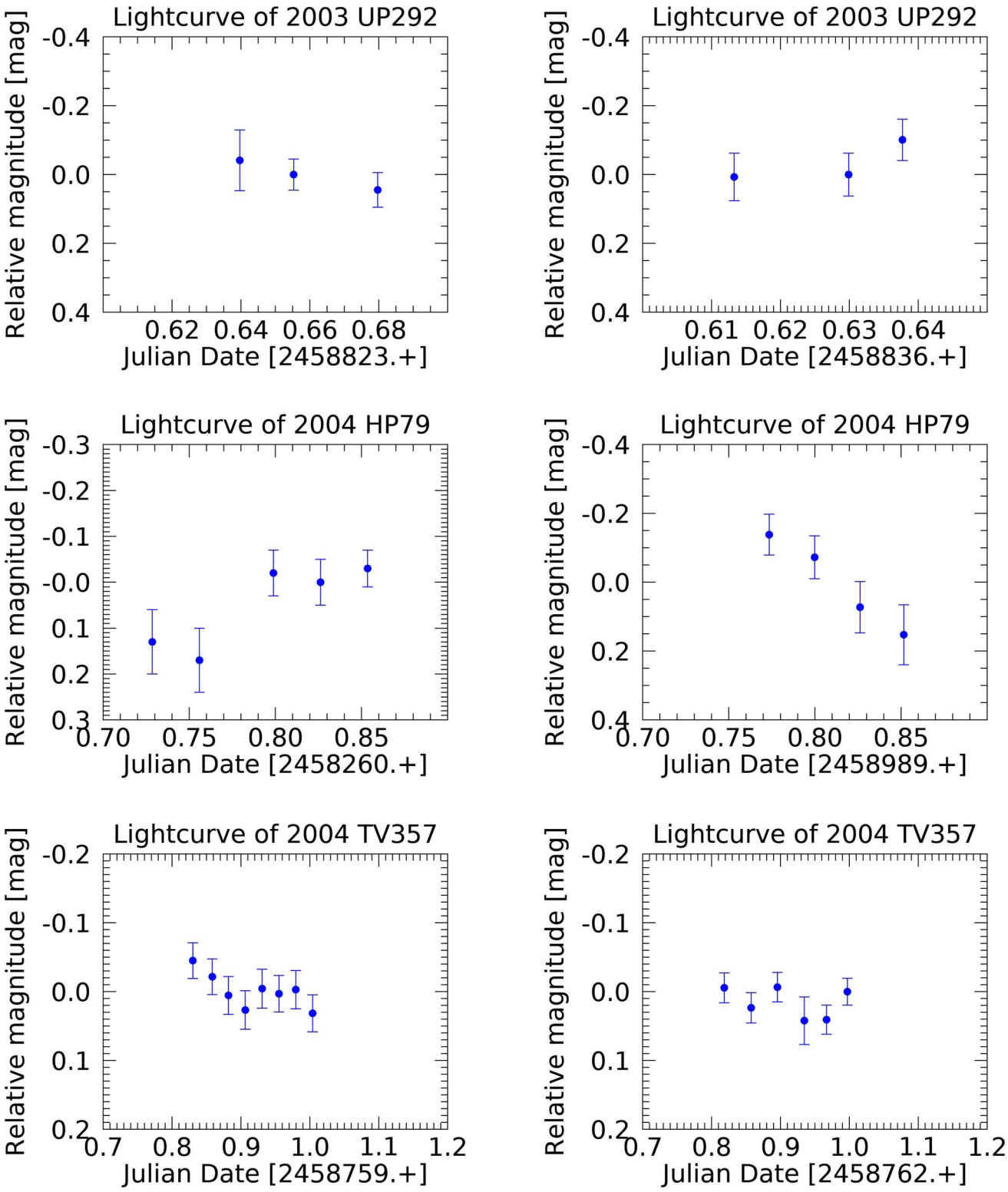

Figure 5. (Continued.)

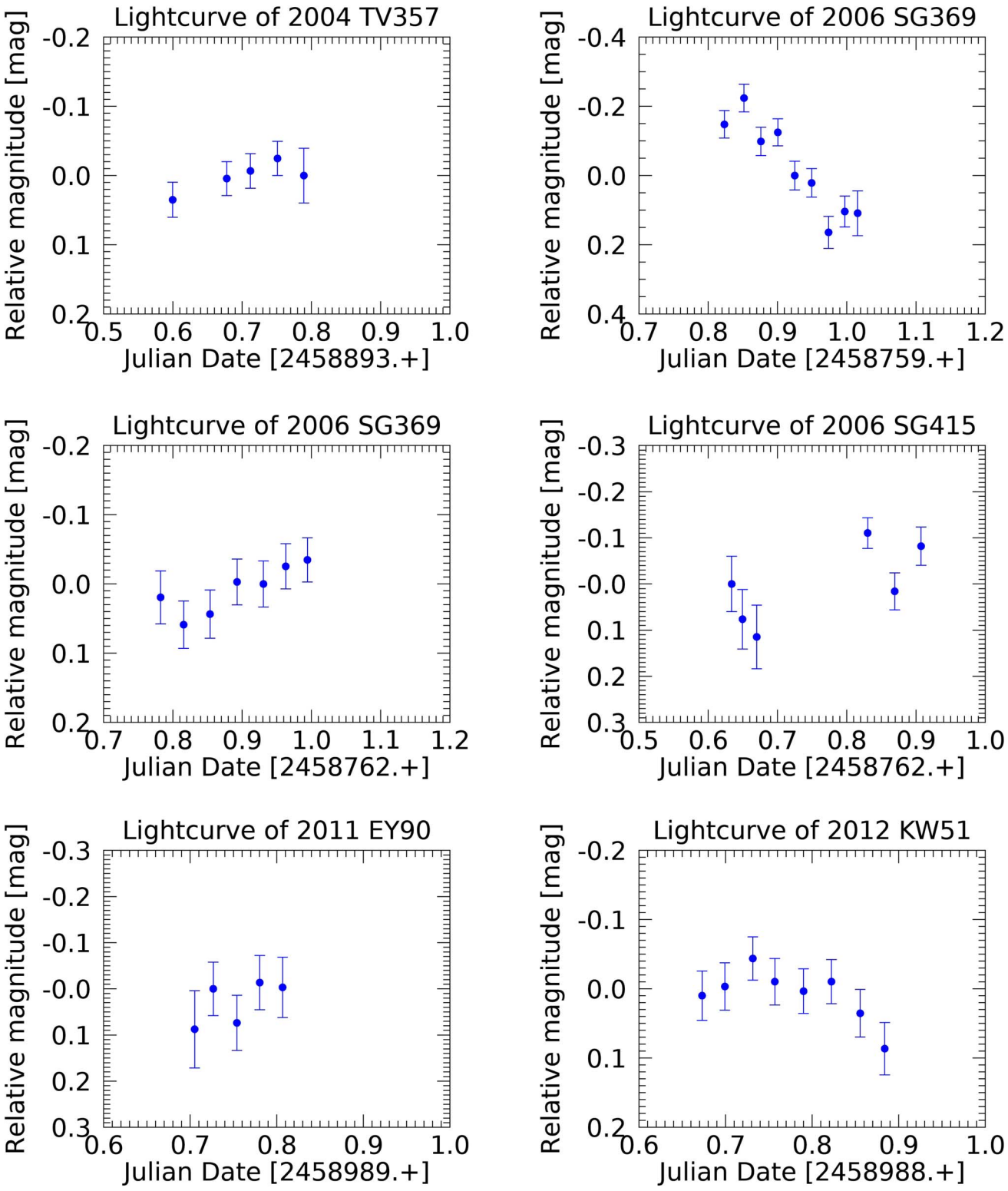

Figure 5. (Continued.)

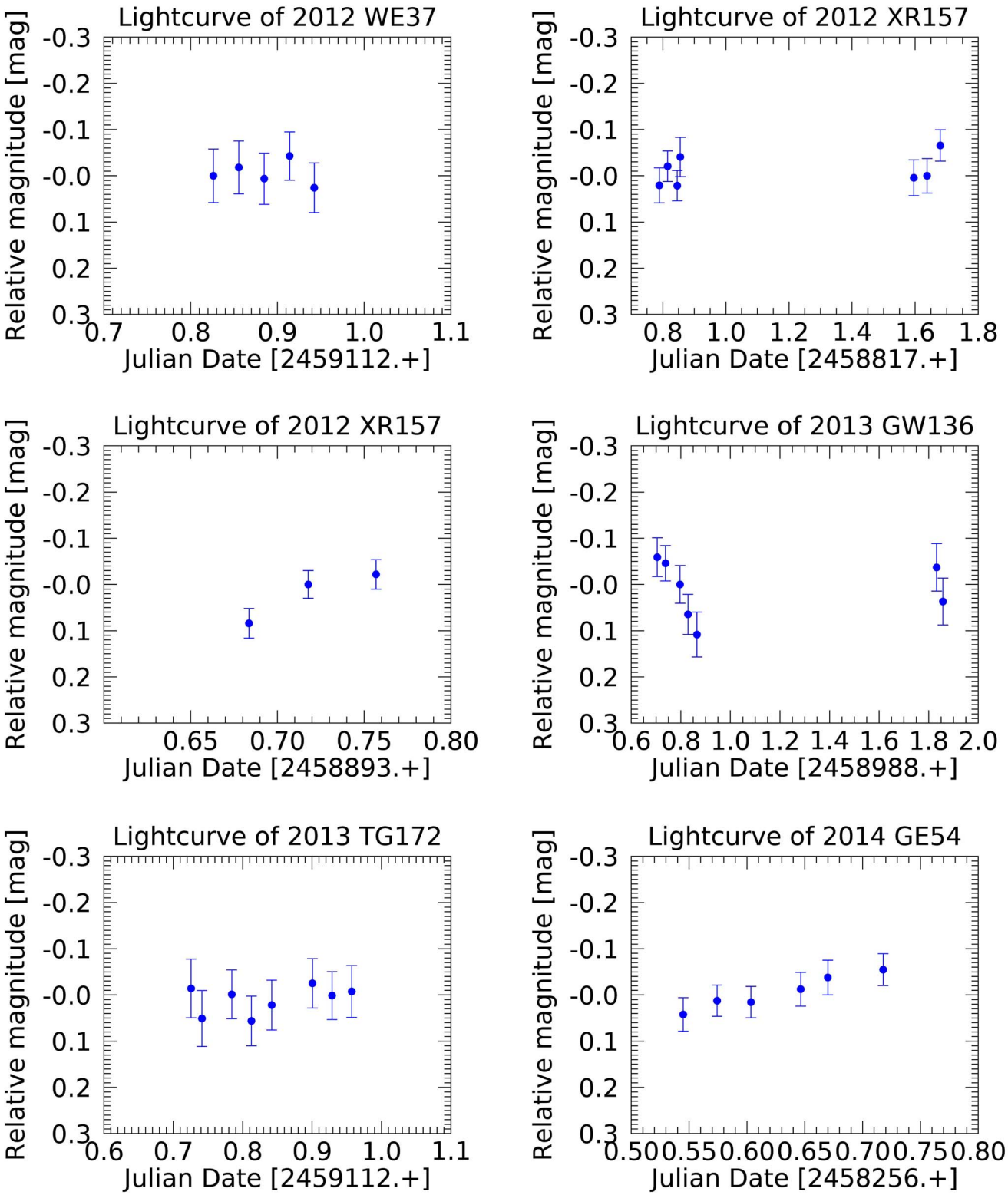

Figure 5. (Continued.)

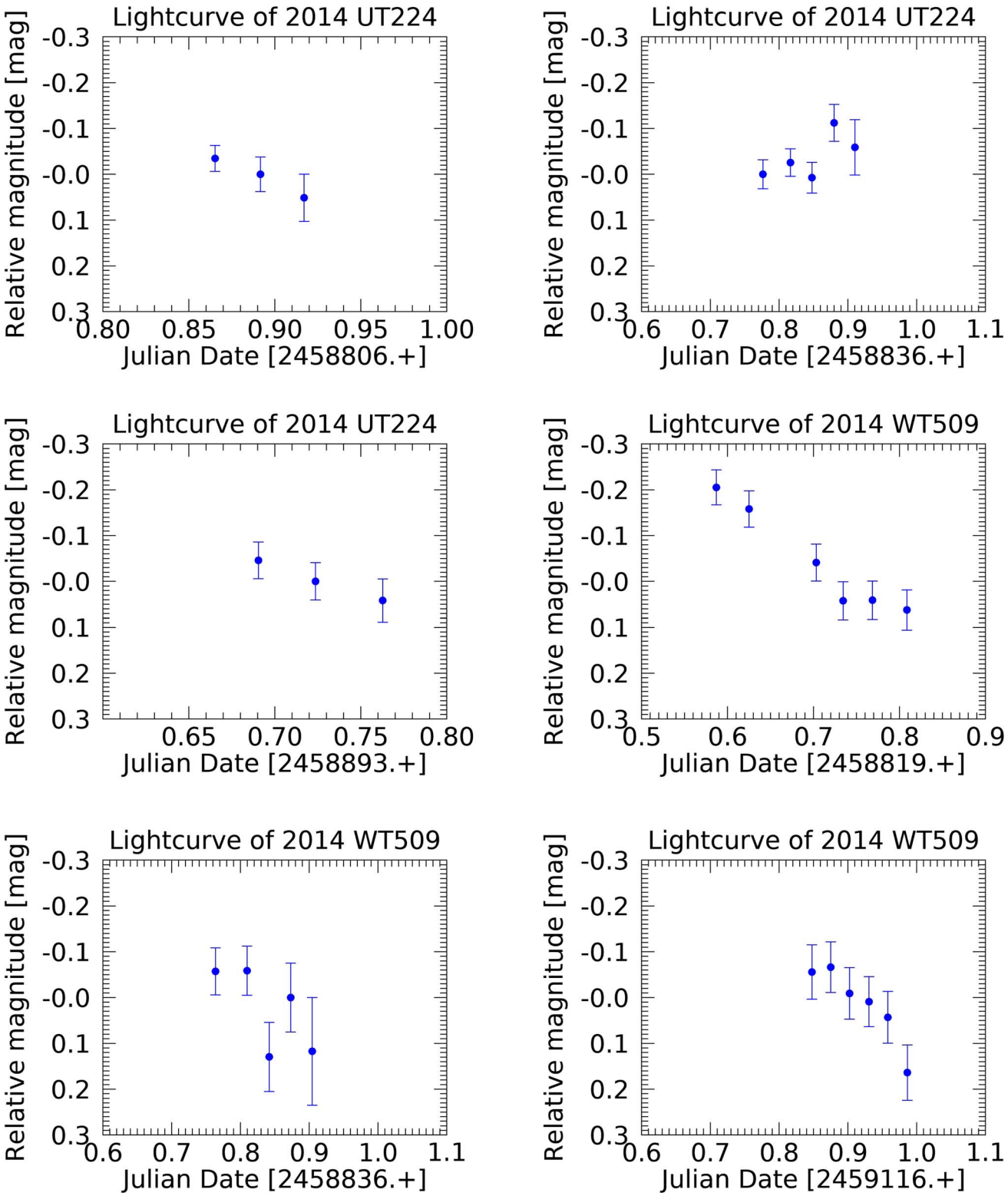

Figure 5. (Continued.)

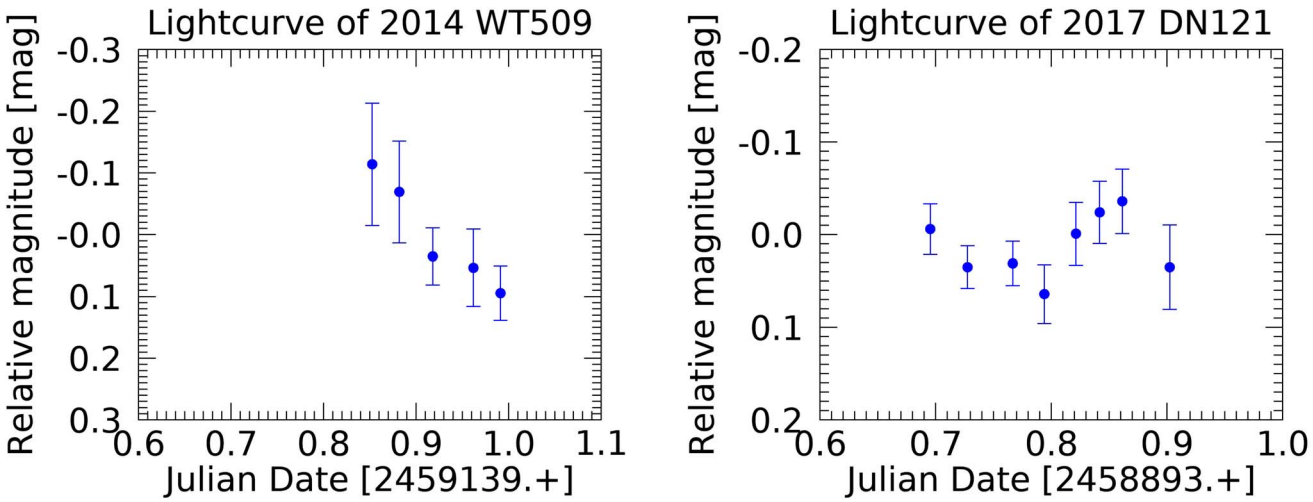

Figure 5. (Continued.)

ORCID iDs

Audrey Thirouin https://orcid.org/0000-0002-1506-4248
Scott S. Sheppard https://orcid.org/0000-0003-3145-8682

References

Abedin, A. Y., Kavelaars, J. J., Greenstreet, S., et al. 2021, AJ, 161, 195
Alexandersen, M., Benecchi, S. D., Chen, Y.-T., et al. 2019, ApJS, 244, 19
Bannister, M. T., Gladman, B. J., Kavelaars, J. J., et al. 2018, ApJS, 236, 18
Benecchi, S. D., & Sheppard, S. S. 2013, AJ, 145, 124
Brown, M. E. 2001, AJ, 121, 2804
Brown, M. E., & Trujillo, C. A. 2002, IAUC, 7807, 1
Chandrasekhar, S. 1969, Ellipsoidal Figures of Equilibrium (New Haven, CT: Yale Univ. Press)
Chandrasekhar, S. 1987, Ellipsoidal Figures of Equilibrium (New York: Dover)
Chen, Y.-T., Gladman, B., Volk, K., et al. 2019, AJ, 158, 214
Delsanti, A. C., Boehnhardt, H., Barrera, L., et al. 2001, A&A, 380, 347
Descamps, P. 2015, Icar, 245, 64
Elliot, J. L., Kern, S. D., Clancy, K. B., et al. 2005, AJ, 129, 1117
Gladman, B., Marsden, B. G., & Vanlaerhoven, C. 2008, in The Solar System Beyond Neptune, ed. M. A. Barucci et al. (Tucson, AZ: Univ. Arizona Press), 43
Goldreich, P., Lithwick, Y., & Sari, R. 2002, Natur, 420, 643
Grundy, W. M., Noll, K. S., Nimmo, F., et al. 2011, Icar, 213, 678
Grundy, W. M., Benecchi, S. D., Rabinowitz, D. L., et al. 2012, Icar, 220, 74
Harris, A., & Warner, B. D. 2020, Icar, 339, 113602
Kern, S. D. 2006, PhD thesis, MIT
Lacerda, P. 2011, AJ, 142, 90
Lacerda, P., & Jewitt, D. C. 2007, AJ, 133, 1393
Lacerda, P., McNeill, A., & Peixinho, N. 2014, MNRAS, 437, 3824
Leone, G., Paolicchi, P., Farinella, P., & Zappala, V. 1984, A&A, 140, 265
Lomb, N. R. 1976, Ap&SS, 39, 447
Morbidelli, A., & Nesvorný, D. 2020, in The Trans-Neptunian Solar System, ed. D. Prialnik, M. A. Barucci, & L. Young (Amsterdam: Elsevier), 25
Murray-Clay, R. A., & Schlichting, H. E. 2011, ApJ, 730, 132
Nesvorný, D. 2015, AJ, 150, 73
Nesvorný, D., & Vokrouhlický, D. 2019, Icar, 331, 49
Nesvorný, D., Youdin, A. N., & Richardson, D. C. 2010, AJ, 140, 785
Noll, K., Grundy, W. M., Nesvorný, D., & Thirouin, A. 2020, in The Trans-Neptunian Solar System, ed. D. Prialnik, M. A. Barucci, & L. Young (Amsterdam: Elsevier), 201
Noll, K. S., Grundy, W. M., Kern, S. D., Levison, H. F., & Stephens, D. C. 2007, IAUC, 8814, 1
Noll, K. S., Stephens, D. C., Grundy, W. M., & Levison, H. F. 2006, IAUC, 8746, 1
Parker, A. H., & Kavelaars, J. J. 2010, ApJL, 722, L204
Peixinho, N., Delsanti, A., & Doressoundiram, A. 2015, A&A, 577, A35
Peixinho, N., Lacerda, P., & Jewitt, D. 2008, AJ, 136, 1837
Petit, J. M., Kavelaars, J. J., Gladman, B. J., et al. 2011, AJ, 142, 131
Porter, S. B., & Grundy, W. M. 2012, Icar, 220, 947
Pravec, P., & Harris, A. W. 2000, Icar, 148, 12
Romanishin, W., Tegler, S. C., Rettig, T. W., Consolmagno, G., & Botthof, B. 2001, PNAS, 98, 11863
Sheppard, S. S. 2007, AJ, 134, 787
Sheppard, S. S. 2012, AJ, 144, 169
Sheppard, S. S., & Jewitt, D. 2004, AJ, 127, 3023
Sheppard, S. S., & Jewitt, D. C. 2002, AJ, 124, 1757
Sheppard, S. S., Lacerda, P., & Ortiz, J. L. 2008, in The Solar System Beyond Neptune, ed. M. A. Barucci et al. (Tucson, AZ: Univ. Arizona Press), 129
Smith, J. A., Tucker, D. L., Kent, S., et al. 2002, AJ, 123, 2121
Spencer, J. R., Stansberry, J. A., Grundy, W. M., & Noll, K. S. 2006, AAS/DPS, 38, 34.01
Stellingwerf, R. F. 1978, ApJ, 224, 953
Thirouin, A. 2013, PhD thesis, Univ. Granada, Spain
Thirouin, A., Noll, K. S., Ortiz, J. L., & Morales, N. 2014, A&A, 569, A3
Thirouin, A., Ortiz, J. L., Duffard, R., et al. 2010, A&A, 522, A93
Thirouin, A., & Sheppard, S. S. 2018, AJ, 155, 248
Thirouin, A., & Sheppard, S. S. 2019a, AJ, 157, 228
Thirouin, A., & Sheppard, S. S. 2019b, AJ, 158, 53
Thirouin, A., Sheppard, S. S., Noll, K. S., et al. 2016, AJ, 151, 148
Vokrouhlický, D., & Nesvorný, D. 2008, AJ, 136, 280
Volk, K., & Malhotra, R. 2019, AJ, 158, 64
Volk, K., Murray-Clay, R., Gladman, B., et al. 2016, AJ, 152, 23
Weidenschilling, S. J. 2002, Icar, 160, 212